VILNIUS UNIVERSITY

INSTITUTE OF THEORETICAL PHYSICS AND ASTRONOMY

Viačeslavas Nelkinas

INVESTIGATION OF THE ELECTRONIC STRUCTURE AND XPS BAND FORM OF CHALCOGENIDES CRYSTALS

Summary of doctoral dissertation

Physical sciences, Physic (02 P)

Vilnius, 2010

The dissertation has been prepared during 2005 – 2010 at Vilnius University

Scientific Supervisor:

Doc. Dr. **Valentinas Rimantas Lazauskas** (Vilnius University Institute of Theoretical Physics and Astronomy, Physical Sciences, Physic – 02 P).

Consultant:

Prof. Habil. Dr. **Jonas Grigas** (Vilnius University, Physical Sciences, Physic – 02 P).

The thesis will be defended at Scientific Board of Physics Faculty.

Chairman:

Prof. Habil. Dr**. Romualdas Karazija** (Vilnius University Institute of Theoretical Physics and Astronomy, Physical Sciences, Physic – 02 P).

Members:

Prof. Habil. Dr. **Algirdas Audzijonis** (Vilnius Pedagogical University, Physical Sciences, Physic – 02 P).
Habil. Dr**. Evaldas Tornau** (Semiconductors Physic Institute, Physical Sciences, Physic – 02 P).
Prof. Habil. Dr. **Antanas Feliksas Orliukas** (Vilnius University, Physical Sciences, Physic – 02 P).
Dr. **Aušra Vektarienė** (Vilnius University Institute of Theoretical Physics and Astronomy, Physical Sciences, Physic – 02 P)

Opponents:

Prof. Habil. Dr. **Jūras Banys** (Vilnius University, Technological Sciences, Material Engineering – 08 T).
Habil. Dr. **Vladimiras Bondarenka** (Semiconductors Physic Institute, Physical Sciences, Physic – 02 P).

The defence of the thesis will take place at the public meeting of the Scientific Board of Physics Faculty on **June 28, 2010** at room 328
Address: A. Goštauto g. 12, 01108 Vilnius, LIETUVA

Summary of the dissertation has been sent on .May 28, 2010.
The thesis is available at the libraries of Vilnius University and Institute of Theoretical Physics and Astronomy.

VILNIAUS UNIVERSITETAS

TEORINĖS FIZIKOS IR ASTRONOMIJOS INSTITUTAS

Viačeslavas Nelkinas

CHALKOGENINIŲ KRISTALŲ ELEKTRONINĖS SANDAROS IR XPS JUOSTŲ FORMŲ TYRIMAS

Daktaro disertacijos santrauka

Fiziniai mokslai, Fizika (02 P)

Vilnius, 2010

Disertacija rengta 2005 – 2010 metais Vilniaus Universiteto Teorinės fizikos ir astronomijos institute.

Mokslinis vadovas:

doc. dr. **Valentinas Rimantas Lazauskas** (Vilniaus Universiteto Teorinės fizikos ir astronomijos institutas, fiziniai mokslai, fizika – 02 P)

Konsultantas:

prof. habl. dr. **Jonas Grigas** (Vilniaus Universitetas, fiziniai mokslai, fizika – 02 P)

Disertacija ginama Vilniaus universiteto Fizikos fakulteto taryboje:

Pirmininkas

prof. habil. dr. **Romualdas Karazija** (Vilniaus Universiteto Teorinės fizikos ir astronomijos institutas, fiziniai mokslai, fizika – 02 P)

Nariai:

prof. habil. dr. **Algirdas Audzijonis** (Vilniaus pedagoginis universitetas, fiziniai mokslai, fizika – 02 P)

habil. dr. **Evaldas Tornau** (Puslaidininkių fizikos institutas, fiziniai mokslai, fizika – 02 P)

prof. habil. dr.. **Antanas Feliksas Orliukas** (Vilniaus Universitetas, fiziniai mokslai, fizika – 02 P)

dr. **Aušra Vektarienė** (Vilniaus Universiteto Teorinės fizikos ir astronomijos institutas, fiziniai mokslai, fizika – 02 P)

Oponentai:

prof. habil. dr. **Jūras Banys** (Vilniaus Universitetas, technologijos mokslai, medžiagų inžinerija – 08 T)

habil. dr. **Vladimiras Bondarenka** (Puslaidininkių fizikos institutas, fiziniai mokslai, fizika – 02 P)

Disertacija bus ginama viešame. **Fizikos fakulteto tarybos** posėdyje 2010 m. birželio 28 d. 15 val. 328 auditorijoje.

Adresas: A. Goštauto g. 12, 01108 Vilnius, LIETUVA

Disertacijos santrauka išsiųsta 2010 m. gegužės 28 d.

Disertaciją galima peržiūrėti Vilniaus Universiteto ir Teorinės fizikos ir astronomijos instituto bibliotekose.

Introduction.

The purpose of the thesis was to study the shape and electronic structure of the valence band (VB) and of core-levels (CL) in the quasi-one-dimensional ferroelectric SbSI and isostructural non-ferroelectric BiSI, SbSeI and quasi-two-dimensional $TlInSe_2$ as well as in the ferroelectric $Sn_2P_2S_6$ crystals by XPS and quantum-mechanical calculations.

X-ray photoelectron spectroscopy is widely used for investigations of the electronic structure of solids. Due to reduced coordination number, the surface atoms experience a different potential than the bulk atoms. Therefore, the core-electron binding energies are different for surface and bulk atoms. XPS enables one to study the surface valence changes, which affect the core-level shift with respect to the bulk atoms. Form and electronic structure of the VB and CL were studied both theoretically and experimentally in the quasi-one-dimensional Sb_2S_3 [1] and Bi_2S_3 [2], SbSI [3], BiSI [4], and SbSeI [5] single crystals. XPS revealed huge crystallographic plane-dependent splitting of the core level binding energies in ferroelectric SbSI, and smaller core-level shifts in non-ferroelectric BiSI and SbSeI. Quasi-one-dimensional crystals attract attention due to “friable” crystal lattice of a complicated chemical bonding and anisotropy of electron and phonon spectra.

Electronic properties of uniaxial ferroelectric $Sn_2P_2S_6$ single crystal are also studied by X-ray photoelectron spectroscopy. XPS of the VB and of the principal CL are obtained from different crystallographic planes in both paraelectric and ferroelectric phases. Ferroelectric phase transition changes atom's charge and bonds strength, VB electronic structure, CL lines width, and chemical shifts for the Sn, P, and S states which are crystallographic plane-dependent.

Theoretical *ab initio* calculations confirmed these findings. The valence band and core levels of these low-dimensional crystals are extremely sensitive to changes of the chemical environment of atoms.

Novelty of the thesis.

For the first time, the electronic structure of the valence band and of the principal core levels of several ferroelectric and isostructural them chalcogenide crystals was studied. The molecular models of the crystals were created for theoretical calculations. The valence band and core levels are revealed experimentally by X-ray photoelectron spectroscopy in the energy range from 0 to 1400 eV and described theoretically. It has been shown how a ferroelectric phase transition changes atom's charge, bonds strength, chemical shifts and the valence band structure, and how the valence band structure is determined by surface and bulk atoms.

Statements presented for defence.

1. The valence band of quasi-one-dimensional ferroelectric SbSI and non-ferroelectric SbSeI crystals is composed of the *s* and *p* bands. The *s* band is formed from the Sb 5*s*, S(Se) 3*s*, and I 5*s* states. The *p* band is formed thoroughly from S(Se) 3*p*, Sb 5*p*, and I 5*p* states. The form of the VB depends on the population of energy levels of surface and bulk atoms.
2. The electronic structure of the valence band and core levels of the quasi-one-dimensional non-ferroelectric BiSI crystals is anisotropic. The form of the valence band and core levels depends on the population of energy levels of surface and bulk atoms.
3. The valence band of quasi-two-dimensional $TlInSe_2$ crystals is composed of the *s* and *sp* bands. Bulk and surface Se 4*s* states form the *s* band. Se 4*p*, In 5*s* and 5*p*, Tl 6*s* and 6*p* states form the *sp* band. The form depends on the population of energy levels of surface and bulk atoms.
4. The electronic structure of ferroelectric $Sn_2P_2S_6$ crystals is anisotropic. The ferroelectric phase transition transforms the electronic structure.

Practical importance of the thesis.

It has been demonstrated how the valence band structure depends on the crystal surface and bulk atom's layers, i.e. how the modification of the crystal surface can change the crystal properties. Investigations of the electronic structure helps better understand the properties of ferroelectric crystals.

The Investigations of the crystals led further theoretical studies at VPU (under the guidance of Prof. A. Audzijonis) and other academic institutions.

Outline of the thesis.

The dissertation consists of introduction, four chapters, conclusions and the list of references.

The motivation of the performed investigation, the aim of the dissertation, solved problems, the novelty of the results, statements presented for defence, and practical importance of the thesis are presented in Introduction.

Chapter 1 is devoted to the review of the research methods. The XPS of valence band and principal core levels were measured using the *PHI 5700/660 Physical Electronics* spectrometer with monochromatic Al K_α radiation (1486.6 eV) of 0.3 eV full width at half maximum. The photoelectron spectra as functions of kinetic energy were analyzed in the 0 - 1400 eV energy range by a hemispherical mirror analyzer. The measurements were performed on the different crystal surfaces all cleaved in vacuum, in the low 10^{-10} torr range, to obtain a clean surface and in a wide temperature range. The survey spectra taken directly after breaking the crystal showed small contamination of carbon that should have no influence on the VB and CL spectra. The angle was 45º between the sample and X-ray incident beam. A charging effect was observed. All spectra were corrected for this charging effect using the carbon 1s line of adsorbed carbon (ε = 284.5 eV).

The calculation method is based on HFR equations in the linear combinations of atomic orbitals (LCAO) approximation for the molecular orbitals (MO). According to the Koopmans' theorem, the one-particle energies obtained from the canonical RHF equations correspond to the approximate energies of the ionization potential. This would be an exact solution if the ionization process was instantaneous and the correlation energy contribution could be completely neglected. Thus, the one-particle picture of many electron molecules in solids is far from being exact. The MO is a linear combination of atomic orbitals (AO)

The MO (φ_i) can be expanded by the AO ($\chi_\mu(\boldsymbol{r})$) base:

$$\boldsymbol{\varphi}_i(r) = \sum_{\mu=1}^{M} C_{i\mu}\boldsymbol{\chi}_\mu(r), \tag{1}$$

where μ is the number of the AO, or the set of quantum numbers *nlm*. For simplicity, a Gaussian 3G orbital basis set [6] is used. The $\boldsymbol{C}$ matrix is obtained by solving Hartree–Fock matrix equation:

$$\boldsymbol{FC} = \boldsymbol{SC\varepsilon}. \tag{2}$$

Eq. (2) is solved by diagonalization as described in [7]. The diagonal matrix ε gives the energies of MO levels. For the core levels they nearly correspond to the energy of the AO levels. However, due to interaction they are slightly diffused. Method of finding the overlap integrals $S_{\mu\nu}$ and the Fock's matrix ($\boldsymbol{F}$) elements is also described in Ref. [7]. The coefficients $C_{i\mu}$ allow to calculate the electronic structure of molecules and to interpret the experimental results. They also allow us to find the matrix of the electron distribution density:

$$P_{\mu\nu} = 2\sum_{i=1}^{N/2} C_{i\mu}C_{i\nu}, \tag{3}$$

which is transformed to the Löwdin density matrix in the following way:

$$P = S^{1/2}PS^{1/2}, \tag{4}$$

or to the Mulliken density matrix in the following way:

$$P = \frac{(SP + PS)}{2}. \tag{4a}$$

The bond strengths P_{AB} between the atoms A and B:

$$P_{AB} = \sum_{\sigma \in A} \sum_{\lambda \in B} P_{\sigma\lambda} \,, \tag{5}$$

and the charge of the atoms:

$$q_A = Z_A - \sum_{\mu \in A} P_{\mu\mu} \,. \tag{6}$$

This method of calculations is realized in GAMESS program [8], which can deal with the molecular objects up to $M \leq 2000$ orbitals or 250 atoms in MINI base. MIDI base is expanded twice for valence electrons and better describes VB, but for core-level electrons the same MINI base remains. We used both MINI and MIDI 3G orbital basis sets. However, for calculating the energy levels we need a molecular model of the crystal.

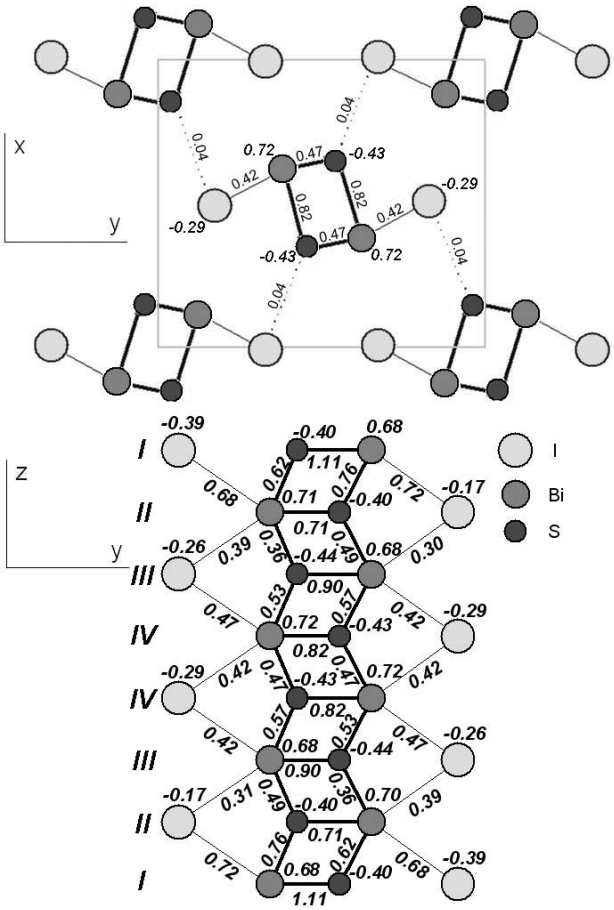

Fig. 1. Crystal structure of BiSI projected on the x–y plane (upper part). The simplified unit cell is formed by 2 BiSI molecules, i.e. by 6 atoms. Molecular chain of BiSI crystal cluster in the zy plane (lower part). The calculated bond strengths and atom's Löwdin charges for 8 (BiSI) cluster are shown in the picture. They are different in different planes along the z-axis and reveal in the.

XPS and electronic structure of quasi-one-dimensional SbSI, SbSeI and BiSI crystals is discussed in **Chapter 2**. BiSI and SbSeI is isostructural to the well-known quasi-one-dimensional ferroelectric (with T_c = 298 K) SbSI, which exhibits a number of strongly coupled semiconductive and ferroelectric properties [9].

Therefore, BiSI and SbSeI crystals are not ferroelectrics in all temperature range, as previously was supposed by some authors [10,11]. For the theoretical *ab initio* calculation of energy levels and for interpreting the experimental results the molecular model of the SbSI type crystal is needed. The model must be a cluster composed of an even number of molecules.

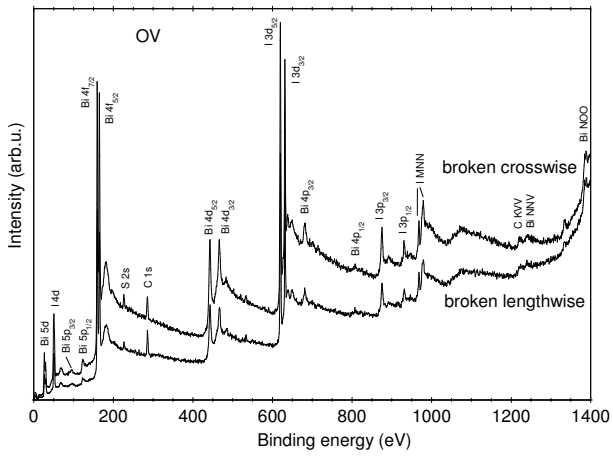

Fig. 2. XPS of BiSI crystal (110) and (001) surfaces in the energy range 0–1400 eV.

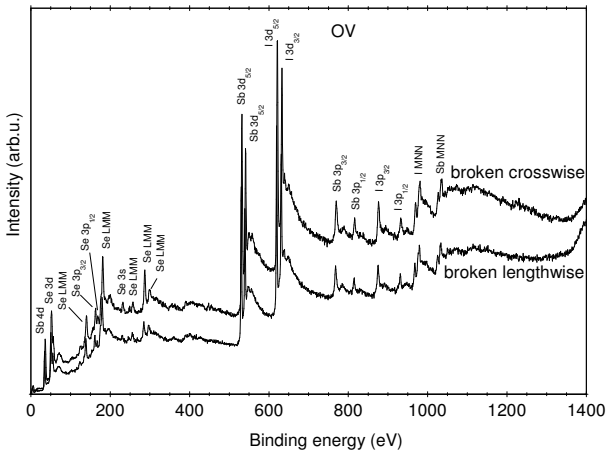

Fig. 3. XPS spectrum of SbSeI in the energy range 0 to 1400 eV. C 1s line is also indicated.

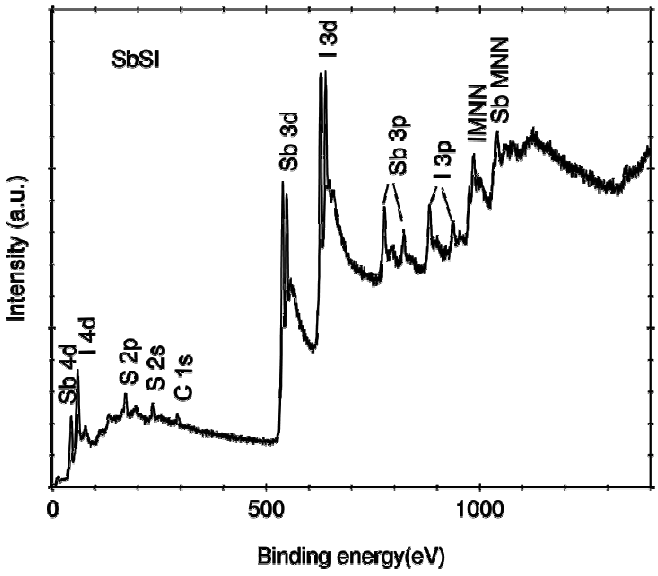

Fig. 4. XPS of SbSI in the energy range of 0 to 1400 eV (the same in FE and PE phases).

The interaction between the clusters is assumed to be weak. A projection of the crystal structure of BiSI on the (110) and (001) planes is shown in Fig. 1. It contains double chains $[(BiSI)_\infty]_2$ consisting of two chains $(BiSI)_\infty$ related by a twofold screw axis and linked together by a short and strong Bi–S bonds [12,13]. Weak van der Waals-type bonds (bond strength 0.04) bind the double chains. The weakly bonded double chains may be considered as non-interacting and one double chain may be taken as a molecular model of the crystal for the binding energies calculation. The double chain is formed of many simplified unit cells. Such a simplified unit cell consists of six atoms. The topology of the crystal is essential for calculations. Extension of the crystal model to several chains results in unstable HFR solutions.

Fig. 2, 3 and 4 shows the XPS of the BiSI, SbSeI and SbSI crystals in the energy range from 0 to 1400 eV below the Fermi level without contamination with any gas and only with a small amount of carbon (C 1s peak at 284.5 eV). Auger spectra of Bi NNV, Bi NOO, I MNN, and of C KVV are seen in Fig. 2. Fig. 3 also shows Auger spectra of Se LMM as well as of Sb MNN and of I MNN, and Fig. 4 - Auger spectra of Sb MNN and of I MNN.

After breaking the crystal under high-vacuum conditions strong bonds of the (0 0 1) surface atoms become open. Due to the reduced coordination number, the (0 0 1) surface atoms experience a different potential than the bulk atoms. As a result, the bond strength of the first two atomic layers from the (0 0 1) surface changes. The bond strength between the first and second atomic layers increases at the expense of broken bonds: it increases in the first layer and decreases in the second one. Table 1 shows Mulliken and Löwdin density matrix approximations of MINI and MIDI bases.

Theoretical HFR calculations express the ionization potential with its zero at the vacuum level, while the experimental binding energies refer to the Fermi level. In order to compare the experimental and theoretical binding energies and to refer to the Fermi level we

Table 1. Atom charges calculated for MINI and MIDI bases. The first column refers to atomic planes.

Base		MIDI		MINI			MIDI		MINI			MIDI		MINI	
Pl	ABC	MUL	LOW	MUL	LOW	ABC	MUL	LOW	MUL	LOW	ABC	MUL	LOW	MUL	LOW
IV	Sb	0,84	0,68	0,77	0,7	Sb	0,62	0,62	0,66	0,6	Bi	0,96	0,84	0,8	0,72
	S	-0,57	-0,42	-0,46	-0,42	Se	-0,43	-0,4	-0,34	-0,31	S	-0,62	-0,52	-0,48	-0,43
	I	-0,29	-0,26	-0,32	-0,28	I	-0,21	-0,22	-0,32	-0,29	I	-0,34	-0,3	-0,33	-0,29
III	Sb	0,81	0,65	0,74	0,67	Sb	0,6	0,59	0,63	0,57	Bi	0,91	0,78	0,77	0,68
	S	-0,57	-0,44	-0,46	-0,43	Se	-0,44	-0,42	-0,36	-0,33	S	-0,62	-0,53	-0,48	-0,44
	I	-0,26	-0,24	-0,3	-0,26	I	-0,19	-0,21	-0,3	-0,27	I	-0,31	-0,28	-0,31	-0,26
II	Sb	0,87	0,68	0,77	0,7	Sb	0,64	0,61	0,66	0,59	Bi	0,96	0,8	0,79	0,7
	S	-0,55	-0,4	-0,43	-0,39	Se	-0,4	-0,36	-0,31	-0,26	S	-0,6	-0,5	-0,46	-0,4
	I	-0,21	-0,17	-0,22	-0,18	I	-0,18	-0,16	-0,23	-0,19	I	-0,26	-0,21	-0,22	-0,17
I	Sb	0,85	0,75	0,71	0,68	Sb	0,73	0,72	0,61	0,59	Bi	0,91	0,85	0,73	0,68
	S	-0,49	-0,4	-0,4	-0,4	Se	-0,37	-0,38	-0,32	-0,32	S	-0,51	-0,46	-0,41	-0,4
	I	-0,44	-0,42	-0,4	-0,39	I	-0,38	-0,39	-0,39	-0,38	I	-0,48	-0,44	-0,4	-0,39

have decreased the calculated ionization potential by the work function. Theoretical calculations explain qualitatively the experimental values of XPS. Nevertheless, the

theoretical eigenvalues of the valence band and core levels are higher than the experimental binding energies (Table 2). Some discrepancy appears because: (i) a limited basis set of AO for obtaining a molecular orbital solution is used (20 BiSI molecules as the crystal model); (ii) screening effects are not taken into account. Nevertheless, Koopmans' theorem provides an invaluable tool in assigning XPS. Calculations of the $C_{i\mu}$ coefficients (Eq. (1)) show that VB consists of s - and p - bands. The longer is the chain, the smaller is the gap between the s- and p-bands. Fig. 5, 6 and 7 shows the theoretically calculated VB form and electronic structure of BiSI, SbSeI and SbSI crystals. The intensities of the XPS were described in three ways:

(a) by the energy states band ε_i from the characteristic Eq. (2);

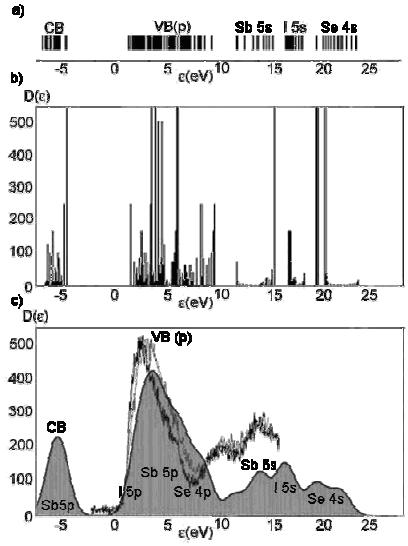

Fig. 5. Electronic structure of VB in SbSeI crystal. Representation for the peaks of the density of states and intensity of the valence electrons for 16 molecules SbSeI cluster (top and middle); VB spectra approximation by the Gaussian broadening method and their comparison with experimental XPS (bottom). Energy states broadening parameter is σ = 0.54 eV.

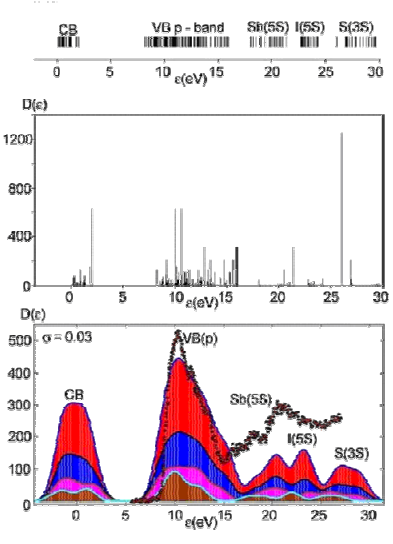

Fig. 6. Electronic structure of SbSI VB. (a) The density of states D(ε) in Eq.(3) representation for the peaks of the density of states of the valence electrons for 16molecules SbSI cluster. (b) VB spectra approximation by the Gaussian broadening method (Eq.(4)) for different SbSI molecular clusters from 2 (lowest curve) to 16 (up per curve) and their comparison with experimental XPS. Energy states broadening parameter is σ =0.54 eV.

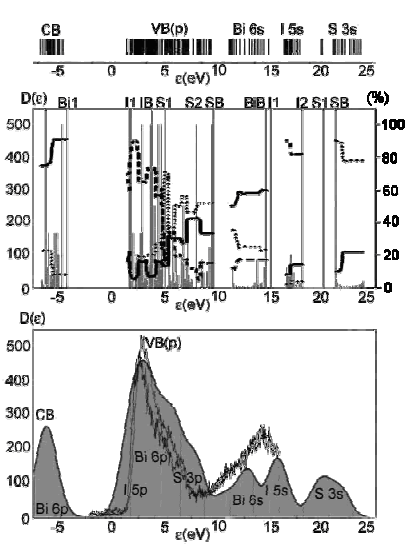

Fig. 7. Electronic structure of BiSI crystal VB. D(ε) is the density of states for 20 (BiSI) cluster; Bi (solid), S (dotted) and I (dashed line) atom electrons contribution (%) to electronic states, as well as the degenerate levels of the first bismuth (Bi1), iodine (I1) or sulphur (S1) and of the second iodine (I2) or sulphur (S2) atomic layers from the (001) surface, and of bismuth, sulphur and iodine bulk states (BiB, SB and IB) are indicated in the middle panel. VB spectra approximation by the Gaussian broadening method and their comparison with experimental XPS are shown in the bottom; the energy states broadening parameter is σ =0.8. CB is the conduction band.

(b) by the peaks of the states density:

$$D(\varepsilon) = \frac{1}{N_M}\frac{1}{\Delta\varepsilon}, \qquad (7)$$

where N_M is the number of molecules in the cluster, $\Delta\varepsilon = (\varepsilon_i - \varepsilon_{i+1})$;

(c) by the Gaussian broadening method [14]:

$$D(\varepsilon) = \frac{1}{\sqrt{2\pi}\sigma}\sum_i \exp(-(\varepsilon - \varepsilon_i)^2 / 2\sigma^2). \qquad (8)$$

where the sum is performed over the states i, ε_i the corresponding energy levels, and σ is the energy broadening parameter.

The Gaussian broadening method is the simplest approach to the Brillouin-zone spectral integrations. The k-points are distributed as evenly as possible throughout the Brillouin zone, and the density of states (DOS) D(ε) is developed according to Eq. (7). This method is designed for an efficient calculation of experimentally observed crystal spectral properties where experimental and lifetime broadenings place a limit on the resolution required. Further, all experiments have a finite-energy resolution and frequently concentrate

Table 2. Theoretical and experimental values of SbSeI, SbSI and BiSI crystals binding energies (eV)

Shell		SbSeI					SbSI					BiSI			
		Eksper.		Theory			Eksper.		Theory			Eksper.		Theory	
		$-E_{max}$	$-E_{min}$	$-\varepsilon_{max}$	$-\varepsilon_{min}$		$-E_{max}$	$-E_{min}$	$-\varepsilon_{max}$	$-\varepsilon_{min}$		$-E_{max}$	$-E_{min}$	$-\varepsilon_{max}$	$-\varepsilon_{min}$
CL	**I 3p**	875	925	894,6	897,5	**I 3p**	880	920	894,6	897,7	**I 3p**	880	930	894,5	897,6
	Sb 3p	760	820	792,7	793,4	**Sb 3p**	770	820	792,9	793,6	**Bi 4p**	680	810	692,9	693,7
	I 3d	619	631	652,1	655	**I 3d**	618	630	652,1	655,2	**I 3d**	619	631	652,0	655,2
	Sb 3d	530	539	564,6	565,3	**Sb 3d**	529	538	564,7	565,5	**Bi 4d**	440	460	485,8	486,7
	Se 3p	160		178	180	**S 2p**	161	162	178	179,7	**S 2p**	230		178,1	179,7
	Se 3d	53	57	66.9	68.9						**Bi 4f**	158,9	164	196,9	197,8
	I 4d	48	52	61,7	64,8	**I 4d**	51	55	61,7	65	**I 4d**	49	50,7	61,6	65,0
	Sb 4d	32	36	49,3	50,1	**Sb 4d**	40		49,4	50,2	**Bi 5d**	25,5	28,5	44,0	45,0
VB s	**Se 4s**			25,2	29	**S 3s**			26	29,4	**S 3s**			26,0	29,5
	I 5s	12	16	21,4	24,1	**I 5s**	12	18	21,4	24,3	**I 5s**			21,2	24,1
	Sb 5s	8	12	17,8	20.9	**Sb 5s**	7,9	12	18	20,9	**Bi 6s**	8	16	17,6	20,6
VB p	**Se 4p**					**S 3p**					**S 3p**				
	Sb 5p	1	8	8,1	15,8	**Sb 5p**	1	7,9	8,2	15,9	**Bi 6p**	1.4	8	8,3	15,7
	I 5p					**I 5p**					**I 5p**				
CB p	**Sb 5p**			2,0		**Sb 5p**			2,0		**Bi 6p**			2,4	

on the shifts, distortions, and changes in weight in the spectral features. In the approach used (Eq. (8)), the aim was to calculate the DOS only at the high density of k-points and then to smear the resulting spectrum to the experimental resolution. However, the application of the Gaussian smearing to the DOS results in a good convergence at low k-point sampling densities. The form of the VB can be explained by the analysis of MO population. Knowing the MO coefficients $C_{i\mu}$ (Eq. (1)), we can evaluate the contribution of the A atom electrons to ε_i state:

$$p_{iA} = \sum_{\mu \in A}^{M} C_{oi\mu}^2 , \qquad (9)$$

where $C_o = S^{1/2}C$ is the matrix of MO coefficients ortogonolized according Löwdin. Fig. 7 gives the comparison of calculated VB structure of BiSI crystal with the experimental XPS spectrum up to 16 eV. At higher energies the VB overlaps with Bi 5d the core level energy (Fig. 2) and is not shown in Fig. 7. Intensity of the bands depends on the DOS. The top of Fig. 7 represents of D(ε) (Eq. (7)) for the peaks of the DOS. In the middle panel of Fig. 7 the DOS and the influence of the electron density of Bi, S and I atoms on states (%) calculated by Eq. (9) is shown. Experimental XPS is the integral picture of all electronic states. At the bottom of Fig. 7 the approximation of BiSI bands spectra by the Gaussian broadening method (Eq. (8)) and their comparison with experimental XPS are

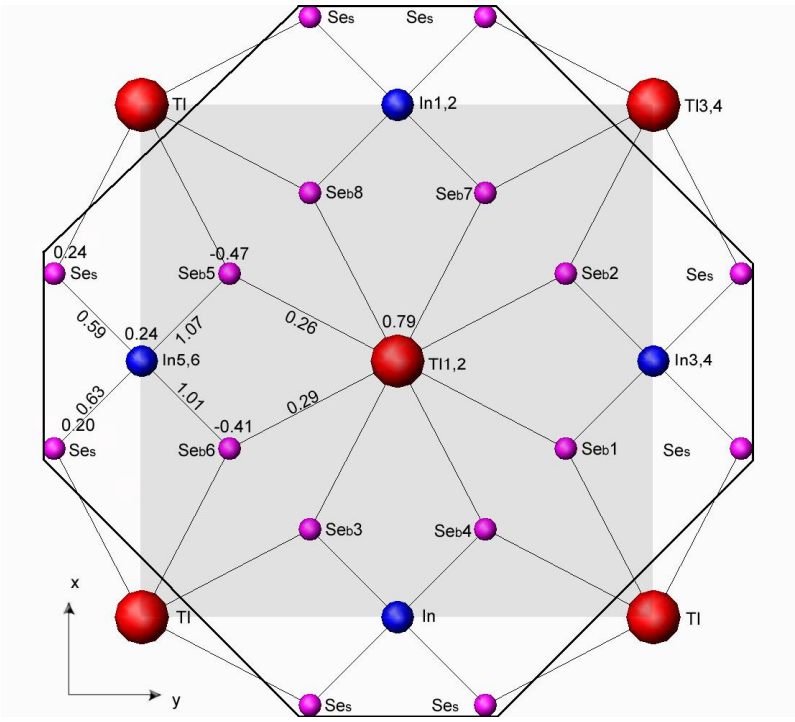

Fig. 8. The $TlIn_4Se_{16}$ cluster as a molecular model (octagon) of $TlInSe_2$ crystal on the xy plane (in shadow). The calculated bond strengths and atom's Löwdin charges are shown in the picture. They are different in different planes from the surface and reveal themselves in the VB and

presented. *Ab initio* calculations give VB p-state broader. This is the shortage of the HFR method due to overestimation of the electron – electron interaction.

XPS and electronic structure of $TlInSe_2$ crystals are described in **Chapter 3**. Low-dimensional chalcogenides are characterized by a "friable" crystal lattice of a complicated chemical bonding. The structural anisotropy affects lattice and electronic properties. Many of them possess various phase transitions, extreme dielectric and electronic properties [9]. The $TlInSe_2$ is a ternary chain crystal [15]. The chain character of its structure derives from the presence of two inequivalent cation sites. In is in a tetragonal site, while Tl is in an octahedral site. The In and Se atoms form covalent chains along the [001] axis. These chains are held together by weaker ionic bonds through the octahedrically coordinated Tl atoms.

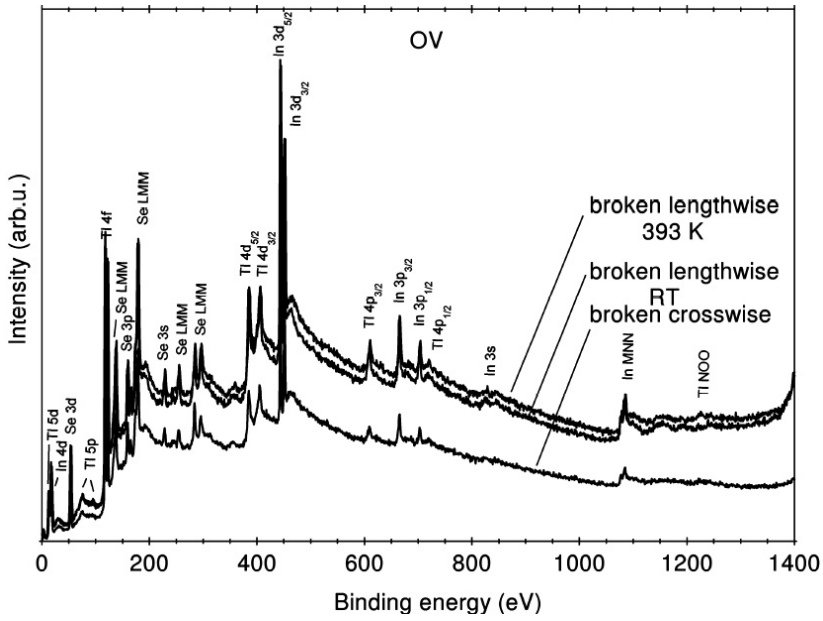

Fig. 9. XPS of $TlInSe_2$ crystal (010) and (001) surfaces in the energy range 0 to1400eV.

The electronic properties of $TlInSe_2$ are strongly influenced by its nearly molecular character. The crystal can be written as $Tl^{1+}(In^{3+}Se_2^{-2})$. This emphasizes that the crystal contains chains of trivalent In covalently bound to Se, which in turn are ionically bound to monovalent Tl. Such chains form a tetragonal lattice of the space group D^{18}_{4h} (I4/mcm). The crystal exhibits many nonlinear effects, such as S-type characteristics with voltage oscillations, switching, and memory, which attract the interest for technological applications

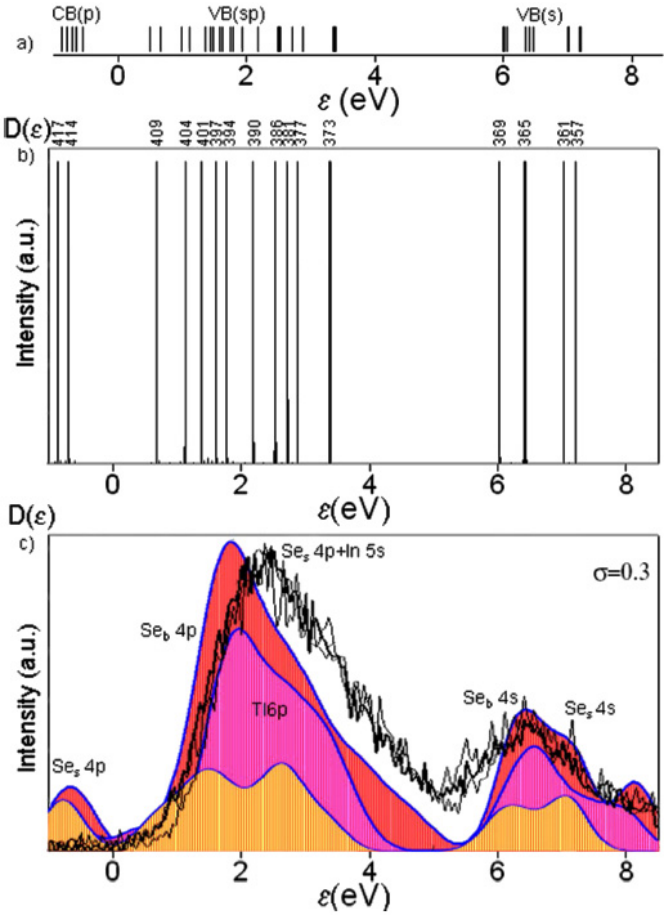

Fig. 10. Electronic structure of VB. DOS band of the $TlIn_4Se_{16}$ cluster (upper panel), intensity of DOS and MOs are indicated in the middle panel. VB spectra approximation by the Gaussian broadening method of three different clusters, $TlIn_4Se_{16}$ (lower part), $Tl_3In_6Se_{24}$ (middle part), and $Tl_7In_{10}Se_{40}$ (upper curve) and their comparison with experimental XPS are shown in the bottom.

Table 3. Mean theoretical values of CL, VB (negative), and CB (positive) binding energies for $TlIn_4Se_{16}$ molecular cluster and experimental values for $TlInSe_2$ crystal.

Band	State	$-\varepsilon_{min} - \varepsilon_{max}$ [eV]	ε (Exp.)[eV]
CL	In 3s	800,3 – 800,3	830
	Tl 4s	724,4 –724,5	
	In 3p	684,5 – 684,6	670 - 710
	Tl 4p	617,0 – 617,1	620 - 730
	In 3d	470,7 – 470,8	444 - 450
	Tl 4d	419,6 – 419,7	390 - 410
	Se 3s	233,6 – 237,3	230
	Se 3p	171,7 – 175,8	160 - 170
	Tl 4f	145,6 – 145,7	118 - 124
	In 4s	131,7 – 131,8	
	Tl 5s	121,7 – 121,8	
	In 4p	91,8 – 91,9	
	Tl 5p	84,3 – 84,4	75 - 100
	Se 3d	60,6 - 64,5	53 -55
	In4d	25,3 –25,6	17 - 20
	Tl5d	22,8 – 23,0	12 - 16
VB(s)	Se 4s	21,5-24,6	5,2 - 10
VB(sp)	In 5s	6,2 - 14,3	0,6 - 5,2
	Se_s 4p		
	Tl 6p		
	Se_b 4p		
CB(p)	Se_b 4p	2,8 - 5,2	

[16, 17]. XPS of binary thallium chalcogenides are discussed in [18]. The electronic structure of $TlInSe_2$ studied by synchrotron radiation photoemission [19] was interpreted in terms of the in equivalent sites for two cations.

The electronic structure of the VB and CL was calculated by the method based on Hartree-Fock (HF) matrix equations solution, in the (LCAO) approach for the molecular orbitals. Figure 8 shows a fragment of the crystal structure on the xy plane. The unit cell is shadowed. It came out that the stable solution gives the quasi-two-dimensional z = 1/4c

plane model. The irreducible cluster of this model is $TlIn_4Se_{16}$. View of the selected cluster $TlIn_4Se_{16}$ of $TlInSe_2$ crystal is framed by an octagon.

Figure 9 shows the XPS of the $TlInSe_2$ crystal in the energy range of 0 to 1400 eV below the Fermi level without contamination by any gas and only with a small amount of carbon (C 1s peak at 284,5 eV). Auger spectra of Se LMM, In MNN, and of Tl NOO are also seen. In elastically scattered electrons give the background. XPS did not show any traces of impurities, only the carbon was visible after the sample was cleft under high vacuum conditions, in the low 10^{-10} torr range. We did not find any noticeable change of the surface composition with time at a given temperature as well as the dependence on illumination time. The strongest peaks of Tl 4f, I 3d, and Se 3d were chosen for investigating peculiarities of the core-level XPS.

Theoretical calculations express the ionization potential with its zero at the vacuum level, while the experimental binding energies refer to the Fermi level. As the energy gap of $TlInSe_2$ is about 0.6 eV, in order to compare the experimental and theoretical binding energies and to refer to the Fermi level we have decreased the calculated ionization potential by the work function $\varphi = 5.2$ eV. Nevertheless, the theoretical eigenvalues of CL differ from experimental ones by about 10% and qualitatively explain the XPS (Table 3). Some discrepancy appears because (i) a limited basis set of AO for obtaining a molecular orbital solution is used (the cluster $TlIn_4Se_{16}$ as the crystal model), (ii) screening and relaxation effects are not taken into account. The relaxation processes are reflected by Auger spectra (Fig. 9). The VB is located at 0.6 to about 10 eV below the Fermi level. The electronic structure of VB is calculated from Eqs. (2). It consists of two bands the intensive sp and less intensive s one. Figure 10 shows the comparison of calculated VB structure of $TlInSe_2$ crystal model with the experimental XPS spectrum up to 10 eV. At higher energies the VB overlaps with the Tl 5d and In 4d core level energies which Kilday et al. [19] have included into VB.

XPS and electronic structure of ferroelectric $Sn_2P_2S_6$ crystals are presented in **Chapter 4**. $Sn_2P_2S_6$ is a well-known uniaxial ferroelectric semiconductor, which exhibits a

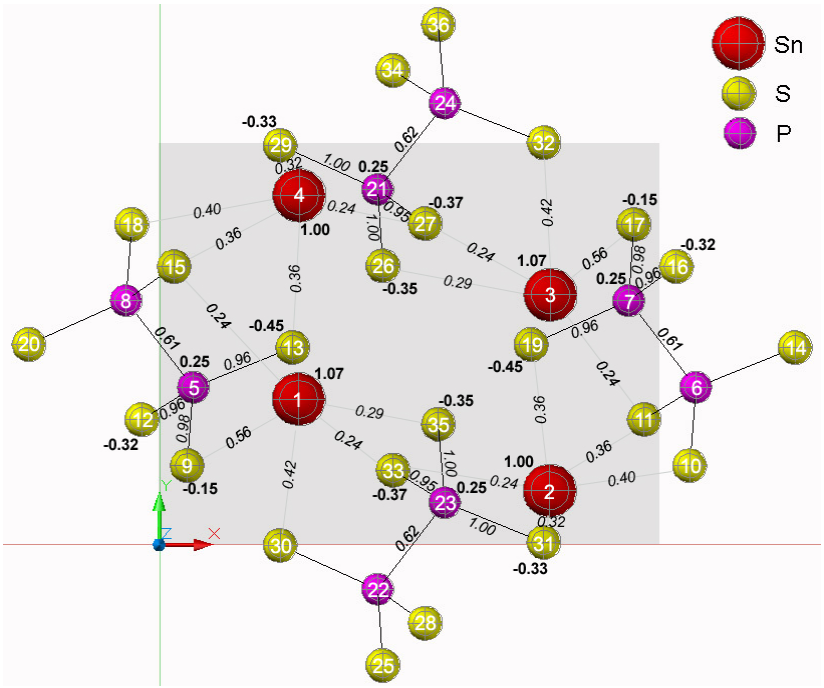

Fig. 11. $Sn_8(P_2S_6)_8$ cluster as a molecular model of $Sn_2P_2S_6$ crystal on the xy plane. The calculated bond strengths and atom's charges in the PE phase are shown in the picture.

number of prominent strongly coupled semiconductive and ferroelectric properties that are discussed in detail in the monograph [20]. The room-temperature ferroelectric (FE) phase is a monoclinic one, with the space group Pc. Above T_c = 337 K, the crystal undergoes a second-order ferroelectric phase transition into paraelectric (PE) monoclinic space group $P2_1/c$. The shapes of the coordination polyhedrons of chalcogen atoms do not differ significantly. Below T_c, all four Sn atoms are shifted significantly in the [100] direction, with respect to the locations in the centrosymmetric state. This is related to nonlinear interaction of soft B_u and full symmetrical A_g modes in the PE phase. This interaction is very important for the phase transition nature. Changes in the position of P and S atoms at T_c are small. Thus, Sn atoms shift mainly along the [100] direction and this allows considering the Sn sublattice as ferroactive one. Ferroelectricity in ferroelectric semiconductors is closely related to their electronic structure [21]. However, electronic properties of this crystal were less studied than structural and phonon properties [20]. Electronic structure of $Sn_2P_2S_6$ so far was studied by X-ray photoelectron spectroscopy in combination with the full – potential linearized augmented plane wave (FLAPW) band structure calculations only in ferroelectric phase [22]. Due to a relative complexity and low symmetry of the crystal, one can expect different XPS from the different crystal planes

(as in SbSI [3]) as well as for the PE and FE phases. We failed to find any studies of the ferroelectric phase transition influence on the electronic structure of this crystal.

Table 4. Sn–S bonds strength in FE and PE phases. Numbers of atoms are given in Fig.11.

Sn-S	FE	PE	Sn-S	FE	PE	Sn-S	FE	PE	Sn-S	FE	PE
1-9	0,41	0,56	2-10	0,55	0,40	3-11	0,19	0,24	4-13	0,23	0,36
1-15	0,10	0,24	2-11	0,48	0,36	3-17	0,50	0,56	4-15	0,35	0,36
1-30	0,42	0,42	2-19	0,45	0,36	3-26	0,05	0,29	4-18	0,32	0,40
1-33	0,38	0,24	2-31	0,36	0,32	3-27	0,07	0,24	4-27	0,46	0,24
1-35	0,43	0,29	2-33	0,10	0,24	3-32	0,28	0,42	4-29	0,33	0,32

Table 5. Values of the calculated and experimental binding (negative) energies (eV).

		FE		**PE**		**Exp.**	
		$-\varepsilon_i$ min	**$-\varepsilon_i$ max**	**$-\varepsilon_i$ min**	**$-\varepsilon_i$ max**		
Sn	**3s**	860,74	859,68	860,31	860,28	875	900
Sn	**3p**	741,21	740,13	740,78	740,73	710	760
Sn	**3d**	520,27	519,19	519,84	519,79	485	497
S	**2s**	246,33	240,17	244,91	241,46	224	228
P	**2s**	210,12	207,90	209,59	208,81	188	191
S	**2p**	182,31	175,99	180,88	177,28	161	164
Sn	**4s**	153,15	152,13	152,75	152,71	136	141
P	**2p**	151,98	149,73	151,46	150,64	131	134
Sn	**4p**	111,22	110,12	110,79	110,70	90	95
Sn	**4d**	40,52	39,42	40,10	39,98	24	28

The calculated bond strengths and the Mullicken charge of the atoms in the PE phase are shown in Fig. 11. In this model, Sn atom's charge is close to +1 and the crystal is ionic $Sn^{+}{}_2(P_2S_6)^{-}$. At the FE phase transition, the bonds strength and charge of atoms change. The greatest changes occur in Sn3 surroundings. These changes are given in Table 4. Those results show that the rearrangement of most of bonds takes place at the ferroelectric phase transition. The valence of ferroactive Sn ions also changes: Sn1 is 3.03 and 2.99, Sn2 is 2.81 and 2.72, Sn3 is 1.92 and 2.99, and Sn4 is 2.81 and 2.72 in the PE and FE phase, respectively.

From the partial density of states (PDOS) (in %) calculated by Eq. (9) and the total density of states (a), the representation D(ε) for the peaks (b) of the DOS (Eq. (7)), and approximation of the bands spectra (c) by the Gaussian broadening method (Eq. (8)) for

Table 6. Binding energies and chemical shifts of atoms at different planes in FE (RT) and PE (360 K) phases.

	Binding energy (eV)					
Peak	RT y,z	360K y,z	RT x,y	360K x,y	RT z,x	360K z,x
P $2p_{3/2}$ in compound	132,0	131,8	132,6	132,1	132,3	131,8
P $2p_{3/2}$ in literature	130,0					
chemical shift	2,0	1,8	2,6	2,1	2,3	1,8
P $2p_{1/2}$ in compound	132,9	132,6	133,5	133,0	133,2	132,6
P $2p_{1/2}$ in literature	131,0					
chemical shift	1,9	1,6	2,5	2,0	2,2	1,6
S $2p_{3/2}$ in compound	162,3	161,9	162,7	162,3	162,4	161,7
S $2p_{3/2}$ in literature	164,0					
chemical shift	-1,7	-2,1	-1,3	-1,7	-1,6	-2,3
S $2p_{1/2}$ in compound	163,5	163,0	163,9	163,5	163,6	162,9
S $2p_{1/2}$ in literature	165					
chemical shift	-1,5	-2,0	-1,1	-1,5	-1,4	-2,1
Sn $3d_{5/2}$ in compound	486,7	486,5	486,9	486,3	486,8	486,3
Sn $3d_{5/2}$ in literature	485,0					
chemical shift	1,7	1,5	1,9	1,3	1,8	1,3
Sn $3d_{3/2}$ in compound	495,1	494,9	495,3	494,7	495,5	494,6
Sn $3d_{3/2}$ in literature	493,0					
chemical shift	2,1	1,9	2,3	1,7	2,5	1,6

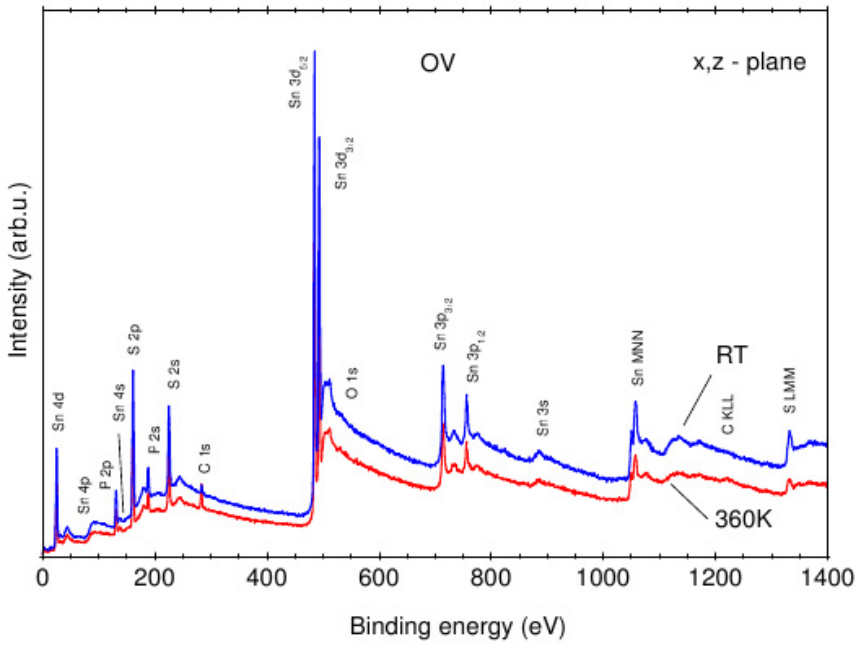

Fig. 12. Overview spectra of $Sn_2P_2S_6$ crystal from the xz plane in the PE (360 K) and FE (RT) phases.

$Sn_4(P_2S_6)_4$ molecular cluster (Fig. 13) it follows that from 4 to 2 eV there is a conduction band (CB), the right edge of which is formed by S 3p electrons. Unlike Sb_2S_3 -

type [1, 2] and SbSI-type [3–5] crystals, the VB consists of five bands. It is dominated by Sn 5s, Sn 5p, S 3s, S 3p, P 3s, and P 3p states. Five DOS peaks are degenerate. The main contribution to the most intensive band between −1 and −5 eV is given by S 3p states. The left edge of this band is formed by S 3p states with 13% Sn 5s and few percent P3p states. The main contribution to the next intensive band between −5 and −12 eV comes from S 3s, S 3p, P 3p, and Sn 5s states. Sn 5s and 5p states give only small contribution to the first two

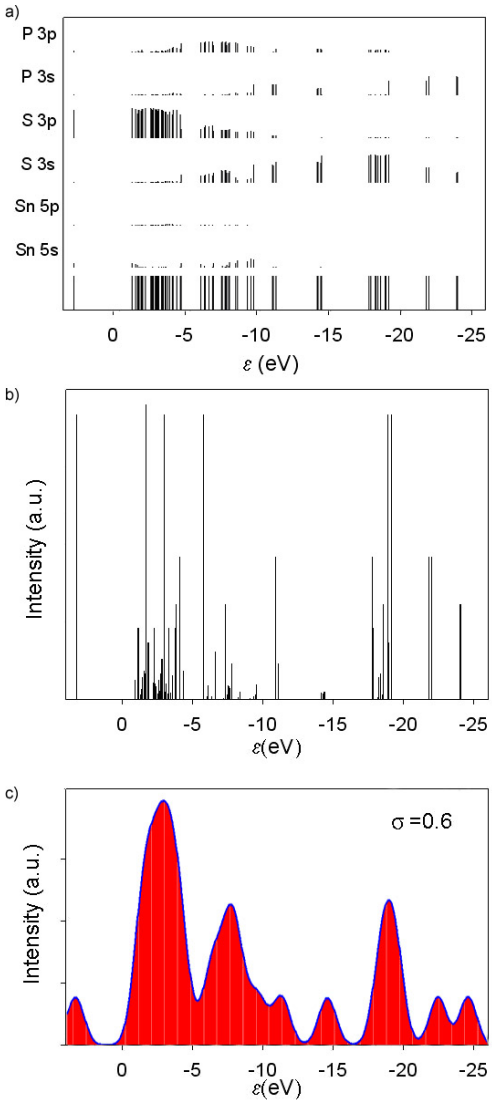

Fig. 13. Electronic structure of VB in PE phase: (a) DOS band and contribution of states (%); (b) intensity of DOS (Δε= 0.27 eV taken in Eq. (6)); (c) calculated VB for $Sn_4(P_2S_6)_4$ cluster and approximated by the Gaussian broadening method (Eq.(7)).

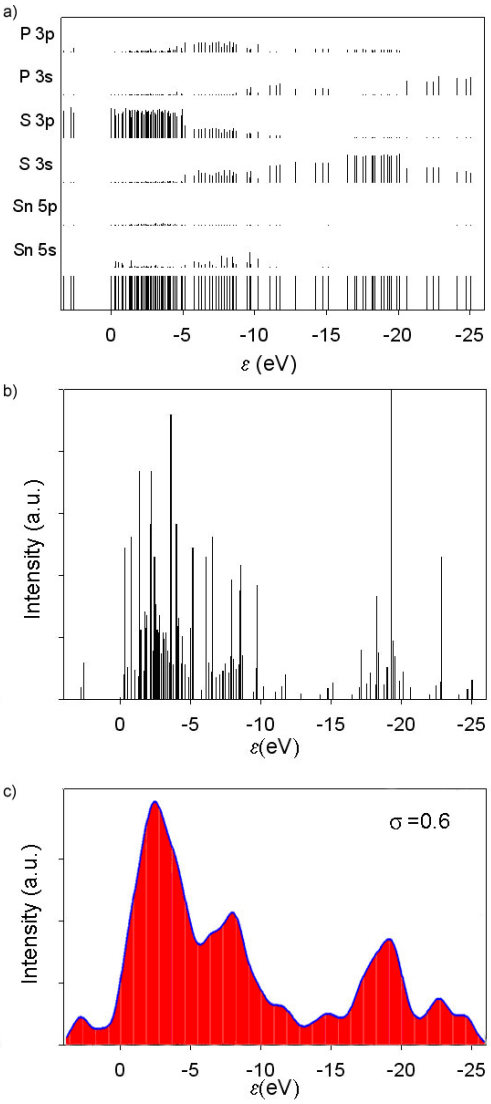

Fig. 14. Electronic structure of VB in FE phase. Designations are the same as in Fig.13. Δε=0.021eV taken in Eq.(6), therefore the intensities are lower and minima are shallower than in PE phase.

bands. The low-energy part of VB is formed mainly by S 3s and P 3s states. S 3s electrons form band at −14 eV, while P 3s electrons form band at −18.5 eV. Above −25 eV dominate P 3s with mixture of S 3s states. The five experimental bands at −3.3, −7.2 ,–9.7, −11.5, and −14.5 eV are in good agreement with [22].

Figure 14 shows the calculated VB form and electronic structure of FE phase. The gap between the VB and CB decreases from 4.1 eV (in PE phase) to 2.6 eV. The calculated width of the VB is 24.9 eV, while in PE phase it is 23.1 eV. In FE phase, there is only one quasi-degenerate state instead of five in PE phase. Disappearance of centro-symmetry lifts degeneracy of the electronic states. The left edge of the most intensive band between −1 and −5 eV is formed by S 3p states with few percent of P 3p states. Sn 5s states disappear. The phase transition does not change essentially the electronic structure of the crystal.

Conclusions

For the first time, the electronic structure, the valence band and core levels form of the series low-dimensional semiconductor ferroelectric and isostructural chalcogenide crystals have been investigated theoretically. The theoretical calculations are confirmed experimentally by X-ray photoelectron spectroscopy. It was found that:

1. The valence band of the quasi-one-dimensional ferroelectric SbSI and non-ferroelectric SbSeI crystals is composed of the *s* and *p* bands. The *s* band is formed from the Sb 5*s*, S(Se) 3*s*, and I 5*s* states. The *p* band is formed thoroughly from S(Se) 3*p*, Sb 5*p*, and I 5*p* states. The form of the VB depends on the population of energy levels of surface and bulk atoms. Se 5*p* states form the conduction band.
2. The electronic structure of the valence band and core levels of the quasi-one-dimensional non-ferroelectric BiSI crystals is anisotropic. The *s* band of the valence band is formed from the 48% Bi 6*s*, 40% S 5*s*, and 12% I 5*s* states. The *p* band is formed thoroughly from 62% I 5*p*, 18% S and 20% Bi states. 90% Bi 6*p* states from firs atomic layer of the surface form the conduction band.

3. The valence band of quasi-two-dimensional $TlInSe_2$ crystals is composed of the *s* and *sp* bands. Bulk 46% and surface 48% Se 4*s* states form the *s* band. Bulk 51% and surface 35% Se 4*p*, In 5*s* and 5*p*, Tl 6*s* and 6*p* states form the *sp* band. Se 4*p* surface states form the conduction band.
4. Ferroelectric phase transition of ferroelectric $Sn_2P_2S_6$ crystals changes atom's charge and bonds strength, valence band electronic structure, core levels lines width, and chemical shifts for the Sn, P, and S states which are anisotropic. Appearance of non-equivalent positions of Sn atoms in ferroelectric phase split the spin–orbit doublets of Sn 3d and 4d spectra.

References

[1] J. Grigas, E. Talik, and V.Lazauskas, X-ray photoelectron spectroscopy of Sb_2S_3 crystals, Phase Transitions **75**, 323 (2002).

[2] J. Grigas, E. Talik, and V.Lazauskas, X-ray photoelectron spectra and electronic structure of Bi_2S_3 crystals, Phys. Status Solidi B **232**, 220 (2002).

[3] J. Grigas, E. Talik, and V.Lazauskas, X-ray photoelectron spectroscopy of ferroelectric semiconductor SbSI crystals, Lithuanian J. Phys. **44**, 427 (2004).

[4] J. Grigas, E. Talik, M. Adamiec, V. Lazauskas, and V. Nelkinas, XPS and electronic structure of quasi-one-dimensional BiSI crystals, J. Electron Spectrosc. and Related Phenom. **153,** 22 (2006).

[5] J. Grigas, E. Talik, M. Adamiec, and V. Lazauskas, X-ray photoelectron spectra and electronic structure of quasi-one-dimensional SbSeI crystals, Cond. Matter Phys. **10**, 101 (2007).

[6] S. Huzinaga (Ed.), *Gaussian Basis Sets for Molecular Calculations*, Elsevier, Amsterdam, 1984, p. 426.

[7] E. Clementi (Ed.), *Modern Techniques in Computational Chemistry*, ESCOM Leiden, 1991, p. 533.

[8] M.W. Schmidt, K.K. Baldrige, J.A. Boatz, S.T. Elbert, M.S. Gordon, J.H. Jensen, S. Koseki, N. Matsunaga, K.A. Nguyen, S. Su, T.L. Windus, M. Dupuis, J.A. Montgomery, General Atomic and Molecular Electronic Strucrure System, J. Comput. Chem. **14** (1993) 1347.

[9] J. Grigas, *Microwave Dielectric Spectroscopy of Ferroelectrics and Related Materials*, OPA Gordon and Breach Science Publ., Amsterdam, 1996, p. 336.

[10] V.M. Fridkin, *Ferroelectric Semiconductors*, Consultants Bureau, New York, 1980, p. 220.

[11] D. Siapkas, Far-infrared reflectivity spectra of BiSI, Ferroelectrics **7,** 295 (1974).

[12] W. Hasse-Wessel, Die Kristallstruktur des Wismutsulfidjodids (BiSJ) Naturwissenschaften **60,** 474 (1973).

[13] Landolt-Börnstein, *BiSI Crystal Structure, Physical Properties*, vol. 41E, Springer-Verlag GmbH, 2000.

[14] C.J. Pickard, M.C. Payne, Extrapolative approaches to Brillouin-zone integration, Phys. Rev. B **59,** 4685 (1999).

[15] G. Margaritondo, in: *Physics and Chemistry of Materials with Low Dimensional Structure – Electronic Structure and Electronic Transitions in Layer Materials: Recent Developments,* Vol. **20**, ed. V. Grasso (Reidel, Dordrecht, 1986) p. 6.

[16] M. Hanias, A.N. Anagnostopoulos, K. Kambas, and J. Spyridelis, I–U dependence of $TlInX_2$ (X = Se, Te) crystals: The ohmic and S-type regions, Phys. Rev. B **43**, 4135 (1991).

[17] C. Karakotsou and A.N. Anagnostopoulos, Crisis in electrical behaviour of the $TlInSe_2$ Semiconducting compound, Physica D **93**, 157 (1996).

[18] L. Porte and A. Tranquard, Spectroscopie photoelectronique (XPS) de calcogenures de thallium, J. Solid State Chem. **35**, 59 (1980).

[19] D.G. Kilday, D.W. Niles, G. Margaritondo, and F.Lewy, Electronic structure of the chain chalcogenide $TlInSe_2$, Phys. Rev. B **35**, 660 (1987).

[20] Yu.M. Vysochanskii, T. Janssen, R. Currat, R. Folk, J. Banys, J. Grigas, and V. Samulionis, *Phase Transitions in Ferroelectric Phosphorous Chalcogenide Crystals* (Vilnius University Publishing House, Vilnius, 2006).

[21] J. Grigas, Splitting of the soft mode in a double well potential of SbSI, Ferroelectrics **226**, 51 (1999).

[22] K. Kuepper, B. Shneider, V. Caciuc, M. Neumann, A.V. Postnikov, A. Ruediger, A.A. Grabar, and Yu.M. Vysochanskii, Electronic structure of $Sn_2P_2S_6$, Phys. Rev. B **67**, 115101 (2003).

List of publications

1. V. Lazauskas, **V. Nelkinas**, J. Grigas, E. Talik, V. Gavriušinas. Electronic structure of valence band of ferroelectric SbSI crystals // Lithuanian Journal of Physics, 2006, vol. **46**, no. 2, p. 205-210.
2. J. Grigas, E. Talik, Adamiec, V. Lazauskas, **V. Nelkinas**. XPS and electronic structure of quasi-one-dimensional BiSI crystals // Journal of electron spectroscopy, 2006, vol. **153**, no 1-2, p. 22-29.
3. J. Grigas, E. Talik, P. Adamiec, V. Lazauskas, **V. Nelkinas**. XPS and electronics structure of $TlInSe_2$ crystals // Lithuanian Journal of Physics, 2007, vol. **47**, no. 1, p. 87-95.
4. J. Grigas, E. Talik, V. Lazauskas, J. Vysochanskii, R. Yevych, M. Adamiec, **V. Nelkinas**. XPS and electronic structure of ferroelectric $Sn_2P_2S_6$ crystals // Lithuanian Journal of Physics, 2008, vol. **48**, no. 2, p. 145-154.
5. J. Grigas, E. Talik, V. Lazauskas, J. Vysochanskii, R. Yevych, M. Adamiec, **V. Nelkinas**. X-ray photoelectron spectroscopy of $Sn_2P_2S_6$ crystals // Condensed matter physics, 2008, vol. **11**, no. 3, p. 473-482.
6. J. Grigas; E. Talik; V. Lazauskas; Yu. M. Vysochanskii; R. Yevych; M. Adamiec; **V. Nelkinas**. XPS of Electronic Structure of Ferroelectric $Sn_2P_2S_6$ Crystals // Ferroelectrics, 2009, vol. **378**, p. 70 – 78.

The results of the thesis were reported in:

1. **V. Nelkinas**, V. Lazauskas, J. Grigas. X-ray photoelectron spectroscopy of $TlInSe_2$ crystal // Advanced materials and technologies : Abstracts book: *The 8-th international summer school-conference*, Palanga, Lithuania, 27-31 August 2006. Kaunas, 2005, p. 47.
2. **V. Nelkinas**, V. Lazauskas, J. Grigas. $Sn_2P_2S_6$ kristalo Rentgeno fotoelektroninio spektro analizė // *37-oji Lietuvos nacionalinė fizikos konferencija* : programa ir pranešimų tezės, Vilnius, 2007 m. birželio 11-13. Vilnius, 2007, p. 152.
3. J. Grigas, E. Talik, V. Lazauskas, J. Vysochanskii, M. Adamiec, R. Yevych, **V. Nelkinas**. XPS of electronic structure of ferroelectric $Sn_2P_2S_6$ crystal // *The 9th Russian-CIS-Baltic-Japan Symposium on Ferroelectricity*, Vilnius, Lithuania, June 15-19, 2008 : Abstracts book. Vilnius, 2008, p. 185.
4. J. Grigas, V. Lazauskas, **V. Nelkinas**. X-ray photoelectron spectroscopy of ferroelectric // Advanced materials and technologies : Abstracts book: *Joint international summer school-conference*, Palanga, Lithuania, 27-31 August 2008, p. 11.
5. V. Lazauskas, **V. Nelkinas**, J. Grigas, Theoretical analysis of photoelectron spectra of $Sn_2P_2S_6$ crystal. // Intern. conf. *Radiation interaction with material and its use in technologies*, 2008, Kaunas, Lithuania, September 24-27, pp. 212-213.

Santrauka

Disertacinį darbą sudaro įvadas, keturi skyriai, išvados, naudotos literatūros sąrašas ir priedai.

Įvade aptartas temos aktualumas, apibrėžti disertacijos tikslai, atliktų tyrimų naujumas, pateikti ginamieji teiginiai, darbo aprobacija bei trumpai išdėstytas disertacijos turinys.

Pirmame skyriuje apžvelgta kvantmechaninio skaičiavimo metodas bei Rentgeno fotoelektroninė spektroskopija (XPS).

Antrame skyriuje interpretuoti išmatuotų SbSeI, SbSI ir BiSI kristalų fotoelektroniniai spektrai, ištirti, kokios kristalo elektroninės posistemės pokyčiai atsispindi XPS, teoriniai rezultatai palyginti su eksperimentinėmis XPS kreivėmis. Tai pat pasiūlyta teoriškai apskaičiuotus spektrus aproksimuoti trimis būdais: elektronų energetinių būsenų juosta, būsenų tankio smailėmis ir aproksimuoti būsenų juostą Gauso funkcijomis. Tirtas elektroninio tankio ryšys su būsenų tankiu. Palyginta SbSI, SbSeI ir BiSI kristalų elektroninė sandara. Identifikuoti valentinės, laidumo ir gilesnių sluoksnių XPS. Skyriuje aptariamos valentinės juostos ir gilesnių būsenų fotoelektronų spektrų formos.

Trečiame skyriuje pateikti $TlInSe_2$ monokristalų Rentgeno spindulių sužadintų fotoelektronų iš (010) bei (001) plokštumų valentinės juostos ir svarbiausių gilių lygmenų spektrai. Eksperimentiškai gautos fotoelektronų energijos palygintos su teorinių *ab initio* skaičiavimų rezultatais. Apskaičiuota ir eksperimentiškai patvirtinta kristalo VB sandara. Parodyta, kokie paviršiaus ir tūrio atomai lemia VB formą. Įvertinti atomų elektros krūviai ir ryšio stipriai. Apskaičiuotasis būsenų tankis ir VB forma artimi eksperimentiškai išmatuotiems. Nustatyti Tl, In ir Se atomų cheminiai poslinkiai.

Ketvirtame skyriuje pateikti ir aptariami Rentgeno fotoelektronų spektroskopija ištirtos elektroninės feroelektrinių $Sn_2P_2S_6$ kristalų savybės. Gauti valentinės juostos ir svarbiausių gilių lygmenų paraelektrinės ir feroelektrinės fazių spektrai nuo įvairių kristalografinių plokštumų. Eksperimentiškai gautos fotoelektronų energijos yra palygintos su teorinių *ab initio* skaičiavimų rezultatais molekuliniam $Sn_2P_2S_6$ kristalo modeliui. Apskaičiuota ir eksperimentiškai patvirtinta kristalo VB sandara abiejose fazėse. Įvertinti Sn, S ir I atomų cheminiai poslinkiai. Ištirta feroelektrinio fazinio virsmo įtaka VB sandarai ir gilių lygmenų spektrams. Nustatyta, kaip fazinis virsmas keičia atomų krūvius, ryšių stiprius, VB elektroninę sandarą ir gilių lygmenų juostų pločius bei Sn, S ir I atomų cheminius poslinkius, kurie priklauso nuo kristalografinės plokštumos.